A&A manuscript no.
(will be inserted by hand later)

Your thesaurus codes are:
06(13.07.1; 13.07.2; 03.19.2; 02.18.5)

ASTRONOMY
AND
ASTROPHYSICS
13.2.1995

COMPTEL observations of the strong gamma–ray burst GRB 940217

C. Winkler[4], R.M. Kippen[3], K. Bennett[4], W. Collmar[1], L.O. Hanlon[4], W. Hermsen[2], K.S. O'Flaherty[4], J. Ryan[3], V. Schönfelder[1], H. Steinle[1], and O.R. Williams[4]

[1] Max–Planck–Institut für extraterrestrische Physik, D–85740 Garching, Germany
[2] SRON–Utrecht, Sorbonnelaan 2, NL–3584 CA Utrecht, The Netherlands
[3] University of New Hampshire, Institute for the Studies of Earth, Oceans and Space, Durham NH 02384, USA
[4] Space Science Department of ESA, Astrophysics Division, ESTEC, NL–2200 AG Noordwijk, The Netherlands

Received: ; accepted:

Abstract. The imaging MeV gamma–ray telescope COMPTEL on board the *Compton* Gamma–Ray Observatory has observed a very strong (S[> 0.3 MeV] = 2.03×10^{-4} erg cm^{-2}), complex, and long lasting (162 s) gamma–ray burst on February 17, 1994 (GRB 940217). The burst consists of several peaks. Temporal fluctuations occur on timescales as short as 100 ms. Hard−to−soft spectral evolution has been observed during the burst emission and also within individual peaks. The photon spectra obtained within the peaks can be modelled by single power law spectra and by broken power laws with break energies at around 1 MeV. The best–fit power law slopes vary between 1.1 and 3.5 throughout the event. The spectra are consistent within COMPTEL's different observing modes and also agree very well with contemporaneous EGRET and BATSE measurements. No significant line emission is detected in any of the recorded spectra. Precise location ($[\alpha_{2000}, \delta_{2000}] = [29.5°, 3.8°]$, with a 3σ error radius of about 1°) has been obtained through direct COMPTEL MeV imaging in combination with timing analysis by the Interplanetary Network. Four hours after the event, the position derived by COMPTEL was distributed to a network of multi–wavelength observers. No detection of a fading or quiescent counterpart has so far been reported at any wavelength. During a 20 minute time interval starting $\sim$ 90 minutes after the burst event, the EGRET instrument on board the *Compton* Gamma–Ray Observatory reported "post–burst" emission at high energies (up to GeV). COMPTEL does not detect any significant "post–burst" emission at low energies (0.3 − 30 MeV), and our upper limits are marginally consistent with the EGRET detections. Using high energy spectral and temporal information, distance limits to GRB 940217 between 145 AU and 11.7 kpc have been derived assuming homogenous and isotropic emission. If GRB 940217 is at cosmological distances (e.g. at 1 Gpc) the lower limit on the relativistic bulk Lorentz beam factor is >18. This implies that our observed breaks at around 1 MeV are either too low in energy to be produced by γ–γ interaction (via e^+e^- – pair creation), or GRB 940217 is closer than 1 Gpc.

Key words: gamma–ray bursts: observations – non-thermal processes

Send offprint requests to: C. Winkler (e-mail [internet]: cwinkler@estsa2.estec.esa.nl)

1. Introduction

The imaging gamma–ray telescope COMPTEL, one of four instruments on board the *Compton* Gamma Ray Observatory (CGRO), has been operating since April 5, 1991. The gamma–ray burst of February 17, 1994 (GRB 940217) was the strongest and one of the longest lasting events observed in the field of view (FOV) of COMPTEL during the first 3 years of operations, therefore rendering it a prime candidate for detailed spectral and imaging investigations. COMPTEL observations of similar events (including e.g. GRB 910425, GRB 910503, GRB 910601, GRB 910814, GRB 930131) have been reported earlier by Winkler et al. (1992a, 1992b, 1992c), Varendorff et al. (1992), Collmar et al. (1992), Connors et al. (1992), Ryan et al. (1994), Hanlon et al. (1994), and Kippen et al. (1994b).

2. Instrument and operating modes

COMPTEL operates in two different modes during the observation of gamma–ray bursts. In its "double scatter mode" (or telescope mode) photons are Compton scattered from one of the upper liquid scintillator detectors over $\sim$ 1.5 m down to one of the lower NaI crystals. This mode allows for the re–construction of the source direction ("direct imaging") within a FOV of ~ 1 sr, provides spectra over $0.75 - 30$ MeV and time histories with 125 μs resolution. In its "single detector mode" two of the lower NaI detectors simultaneously accumulate spectra in two energy ranges $0.1 - 1.5$ MeV (122 channels) and $0.2 - 10$ MeV (128 channels), respectively. However, reliable detector response information (see Section 3.2.2) is only available for energies $E > 0.3$ MeV (low range) and $E > 0.6$ MeV (high range). The sequence of accumulated burst spectra in those detectors is initiated by receipt of a BATSE trigger signal. In the default mode, prior to the trigger, background spectra (100 s integration time each) are recorded until this sequence is interrupted by the receipt of the BATSE trigger signal and subsequently 6 spectra (each of 1 s integration time), followed by 133 spectra (each of 6 s integration time) are accumulated. Finally the background mode is re–entered awaiting the next BATSE trigger. Spectral resolution for both modes is $< 9.5\%$ ($E > 0.5$ MeV). A detailed description of the COMPTEL instrument can be found in Schönfelder et al. (1993).

3. Observational data and results

On February 17, 1994 (Truncated Julian Day (TJD) = 9400) at UT = 82962 s, an outburst of celestial high energy gamma radiation was reported by BATSE (trigger # 2831) which triggered the "single detector mode" of COMPTEL, while a total of ~ 740 photons were obtained in the "double scatter mode".

3.1. Time histories

Deadtime corrected lightcurves from the event are shown for different energy ranges in Figures 1 and 2. The burst emission commences ~ 6 seconds after the onset (at UT = 82962 s) and largely consists of 6 well separated peaks (Table 1) with a total duration of 162 s.

Table 1. GRB 940217: Time intervals used for spectral analysis (see Figures 1 and 2). T_{start} = start of the integration time of "single detector mode" spectra.

Peak #	T_{start} (s)	Duration (s)
Full burst	82962.12	162
1	82968.21	30
2	83022.44	6
3	83046.56	18
4	83070.66	12
5	83088.75	18
6	83112.87	12

We note already from Figures 1 and 2, that the relative peak amplitudes vary with energy indicating different spectral shapes of individual peaks (see also Section 3.2 and Figures 3 and 6).

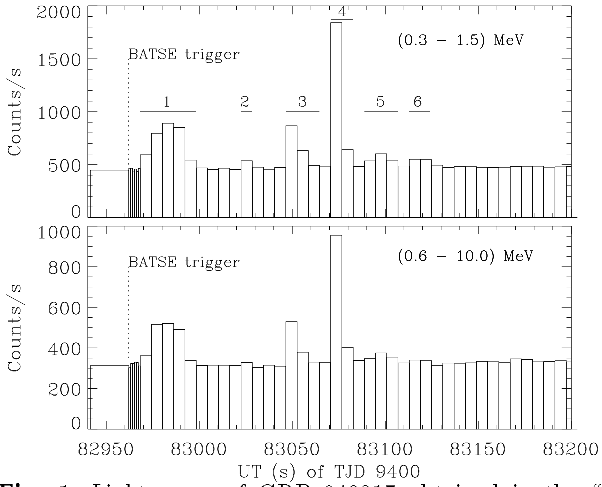

Fig. 1. Lightcurves of GRB 940217 obtained in the "single detector mode", upper panel = low energy range, lower panel = high energy range. Time intervals containing peaks #1 – #6 used for spectral deconvolution of both ranges are indicated.

The "double scatter mode" (telescope) lightcurve was examined by binning the events on smaller and smaller time scales until significant variation was no longer visible. The fastest temporal variations have a full width of ~ 100 ms. Several of these occurred throughout the burst, the shortest is within analysis peak #4 (Figure 2, inset).

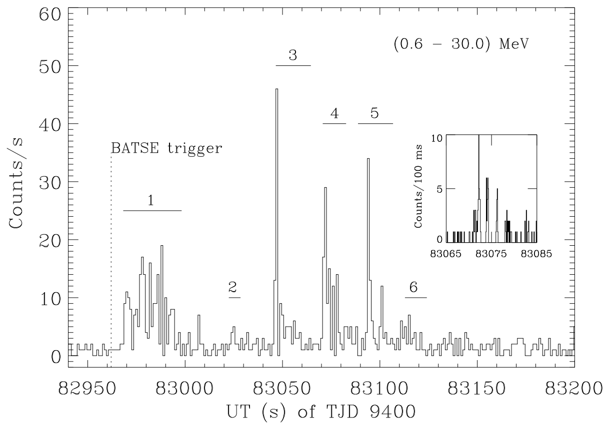

Fig. 2. Lightcurve of GRB 940217 obtained in the "double scatter mode" with 1 s binning. Time intervals containing peaks #1 – #6 used for spectral deconvolution are indicated and are identical to the ones shown in Figure 1. The inset displays fast temporal variations with 100 ms binning during peak #4.

3.2. Spectral analysis

3.2.1. Spectral evolution

Hardness ratios (Figure 3) were computed for all spectra obtained in the "single detector mode" and within all the 6 lightcurve peaks (Figure 1). We used background subtracted counts from two energy ranges (0.1 − 0.3 MeV and 0.3 − 1.5 MeV) of the low range detector. In general, hardness ratios from this detector have better statistics compared to those derived using data from the high and low range detectors. The background was determined by fitting a 2nd order polynomial to the 0.1 − 1.5 MeV data (see Section 3.2.2). Each data point in Figure 3 represents a 6 s integration time. We note an overall trend of hard−to−soft evolution both within individual peaks and from peak to peak. A least squares fit to the data shows significant deviation (12.4σ) from a line of zero slope, although this fit is formally only a poor model of the hardness evolution (χ^2 = 227 for 14 d.o.f.). Apart from the global trend we note that peak #1 becomes harder after 6 s followed by a softening. Peak #4, the last 12 s of peak #5 and peak #6 also show softening. Peak #2 is relatively soft before the burst apparently gets harder again at the onset of peak #3. Besides the general hard−to−soft evolution described above, the data alternatively suggest a "2−fold" evolution consisting of peaks #1 and #2, and peaks #3 to #6 (Figure 3). Again, the slope of each subset deviates significantly from a flat hardness ratio.

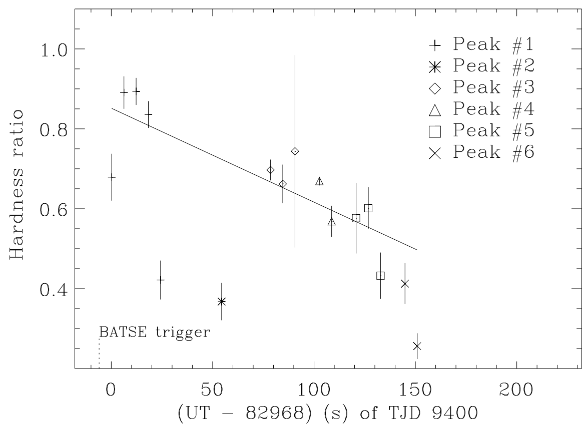

Fig. 3. Hardness ratios for GRB 940217. The hardness ratio was calculated using background subtracted counts from low range data ([0.3 − 1.5 MeV]/[0.1 − 0.3 MeV]) in "single detector mode". Statistical error bars shown are 1σ.

3.2.2. Photon spectra

Single detector mode The count spectra obtained in "single detector mode" were processed as follows: a background was subtracted from all deadtime corrected and energy calibrated spectra. This background is estimated from the observed background spectrum (100 s integration time) obtained prior to the burst onset multiplied by a time dependant scaling function to account for the (mainly orbital) long–term temporal variation of the background during the burst emission. The scaling function was determined by fitting the background, excluding the period of burst emission (162 s duration), with a polynomial: the long term trend in the background (outside the time interval shown in Figure 1) is energy dependant and has been fitted with a 1st order polynomial for the low range data, and with a 2nd order polynomial for the high range data. The spectral fitting of these background subtracted data was performed using a standard forward folding technique of convolving a trial photon spectrum with the detector response matrix, covering both ranges, into a count spectrum. The two energy ranges were treated individually. The location of the burst (see Section 3.3.1) in the instrument coordinate system (zenith = 10.35°, azimuth = 308.93°) was used in calculating the effective detector area. The convolved trial photon spectrum was then compared with the observed spectrum in count space and a minimum χ^2 was iteratively determined for the best–fit photon spectrum. A single power law spectrum was used as the trial input. In this model, the photon flux is given by $a \times$ E$^{-\alpha}$ with normalization a [photons/(cm^2 s MeV)] at 1 MeV, energy E [MeV], and slope α.

In the case that the hypothesis of a single power law could not be accepted (on >5% level) because of too large χ^2 values, the fit was repeated using a broken power law model with 4 parameters a (as above), break energy E_{break} [MeV], and power law slopes α_{low} and α_{high} below and above E_{break}, respectively.

The errors on the best–fit parameters were estimated using the prescription given by Lampton et al. (1976): following their Table 1, 90% confidence intervals (1.6σ) for the parameters fitted simultaneously were obtained by using the parameter space between χ^2_{min} and $\chi^2_{min} + \Delta$, where Δ = 4.61 for 2–parameter fits (single power law) and Δ = 7.78 for 4–parameter fits (broken power law).

Prior to spectral fitting, the background subtracted spectra were rebinned in order to ensure that each bin contains a sufficient number of counts to validate the application of χ^2 statistics. Starting from the high energy end of the spectral range the energy bins were combined until the number of counts in the new bin exceeds the background by 3σ. In general this results in an energy dependant bin size, with the bin size increasing with energy.

χ^2 tests were applied in the energy ranges 0.3 − 1.5 MeV for low range spectra, and 0.6 − 10 MeV for high range spectra. The energy ranges are determined by the boundaries of the available energy response matrix information (see Section 2).

Detailed results obtained by fitting trial photon spectra to both ranges are shown in Table 2 (single power laws) and Table 3 (broken power laws). The majority of the fitted photon spectra can indeed be described by single power laws with slopes ranging from $\alpha = 1.78^{+0.52}_{-0.38}$ (peak #5) to $\alpha = 3.52^{+0.88}_{-1.00}$ (peak #2). A least squares fit to the data (power law slopes vs. time) of Table 2 shows a 2.6σ deviation from a flat line.

The high range data for peaks #1, #4 and for the full burst duration fail to accept the hypothesis of a single power law model and require a broken power law fit with break energies at around 1 MeV. High range data for peaks #2 and #6 could not be used for spectral deconvolution, because due to the low flux (cf. Figure 1), the 3σ–rebinning (see above) resulted in a small number of energy bins which was insufficient for spectral fitting. As an example the photon spectrum for the full burst event (162 s, Tables 2 and 3) is shown in Figure 4.

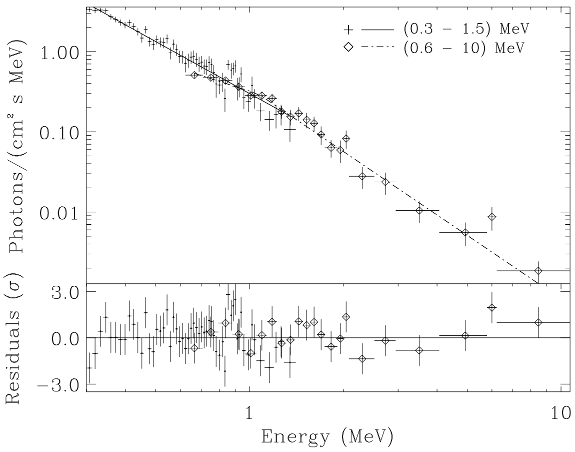

Fig. 4. Photon spectrum of GRB 940217 (full burst, 162 s duration) obtained in "single detector mode". The solid line is the best–fit single power law to low range $0.3 - 1.5$ MeV data with normalization $a = 0.30 \pm 0.02$ photons/(cm^2 s MeV), and slope $\alpha = 2.15 \pm 0.12$. The dashed line is the best–fit broken power law to high range $0.6 - 10.0$ MeV data with $a = 0.32^{+0.09}_{-0.06}$ photons/(cm^2 s MeV), and slopes $\alpha_{\rm low} = 1.25^{+0.85}_{-1.20}$ and $\alpha_{\rm high} = 2.63^{+0.77}_{-0.35}$ below and above the break energy $E_{\rm break} = 1.07^{+0.75}_{-0.35}$ MeV, respectively.

Double scatter mode The telescope $0.75 - 30$ MeV data were fitted within the same intervals (peaks) as used for the "single detector mode" data (Table 1, Figures 1 and 2). Here, a single power law photon spectrum with slope $\alpha = 2.0$ was simulated at the proper burst position (see Section 3.3.1) in order to determine the instrument energy response function. The response is found to be insensitive to the exact shape of the trial spectrum (provided the energy bins are larger than the instrument resolution). By selecting only those events which originate close to the derived source direction, photons which are incompletely absorbed in the lower detector are eliminated (Schönfelder et al. 1993). This selection results in three main effects: (i) the energy response matrix is (nearly) diagonal which reduces matrix inversion to scalar multiplication; (ii) the background is significantly reduced; (iii) the detection efficiency is reduced. This simulated energy response matrix is used to calculate the burst photon flux from the observed (deadtime corrected) count spectrum.

The standard COMPTEL event selection criteria applied include those for pulse shape, time–of–flight and energy (see Schönfelder et al. 1993 for a detailed description), as well as the additional constraint to select only those events within 10° of the derived burst location.

Model testing is performed by forward folding spectral models and comparing the model counts with the background (measured 15 orbits or $\sim$ 84000 s later) and with the observed data in count space. The Cash statistic (Cash 1976) is used to estimate model parameters and their uncertainties. This statistic cannot be used to directly derive a "goodness of fit" value, therefore random bootstrap simulation is applied. In each simulation, the best–fit model counts are randomized (poisson–distributed) and the Cash statistic is evaluated between the randomized spectrum and the best–fit model. For many such random samples this forms a distribution of Cash statistics which are due only to random deviations of the model. By examining where the Cash statistic of the observed data with the best–fit model falls in this distribution, we can determine if the data are consistent with the model ("goodness of fit").

The parameter of interest is the fraction of random samples with Cash statistics greater than that of the observed data. This is just the probability (Π) of observing a Cash statistic greater than that of the real data based only on random fluctuations of the model. This is equivalent to the probability of observing $\chi^2 > \chi^2_{\rm min}$ implying that we can reject models with $(1 - \Pi)$ confidence, but in general we expect $\Pi \sim 0.5$ which corresponds to $\chi^2/\nu = 1$.

We tested single power law, optically thin thermal bremsstrahlung (OTTB) and thermal synchrotron models. Single power laws are acceptable for all phases of the burst, and no broken power laws are required in the 0.75 – 30 MeV energy range. OTTB models can be rejected for the full burst, and for peaks #5 and #6. Synchrotron models can be rejected for the full burst and for peaks #4, #5 and #6.

Spectral fitting results using telescope ("double scatter mode") data are shown in Table 4. Errors on fit parameters are 90% confidence (1.6σ). Uncertainties in deadtime estimates lead to systematic normalization errors of up to 50%. The telescope photon spectrum for GRB 940217 (full burst duration of 162 s) is shown in Figure 5. The errors shown in Figure 5 are derived during the fitting process and are statistical errors only.

Comparison of Table 4 with Tables 2 and 3 and comparison of Figure 5 with Figure 4, shows very good agreement between the independent data obtained in the two

Table 2. GRB 940217: Single power law photon spectra ("single detector mode").

Time interval (see Table 1)	Range MeV	normalization a photons/(cm^2 s MeV)	slope α	$\chi^2_{\rm d.o.f.}$	d.o.f.	Notes
Full burst	0.3 − 1.5	0.30 ± 0.02	2.15 ± 0.12	68.2	54	
Full burst	0.6 − 10.0	–	–	–	–	(a)
Peak #1	0.3 − 1.5	0.63 ± 0.04	1.86 ± 0.11	74.3	62	
Peak #1	0.6 − 10.0	–	–	–	–	(a)
Peak #2	0.3 − 1.5	$0.07^{+0.07}_{-0.04}$	$3.52^{+0.88}_{-1.00}$	3.4	4	
Peak #2	0.6 − 10.0	–	–	–	–	(b)
Peak #3	0.3 − 1.5	$0.41^{+0.04}_{-0.55}$	2.07 ± 0.20	37.2	39	
Peak #3	0.6 − 10.0	0.37 ± 0.05	$2.29^{+0.26}_{-0.19}$	16.0	12	
Peak #4	0.3 − 1.5	1.51 ± 0.08	2.20 ± 0.08	86.3	70	
Peak #4	0.6 − 10.0	–	–	–	–	(a)
Peak #5	0.3 − 1.5	$0.18^{+0.04}_{-0.06}$	2.15 ± 0.48	11.8	14	
Peak #5	0.6 − 10.0	0.11 ± 0.05	$1.78^{+0.52}_{-0.38}$	6.9	4	
Peak #6	0.3 − 1.5	$0.07^{+0.05}_{-0.04}$	3.30 ± 0.70	7.1	8	
Peak #6	0.6 − 10.0	–	–	–	–	(b)

Note: Errors on fit parameters are 90% confidence intervals (1.6σ).
(a): see Table 3 for broken power law fit
(b): see text

Table 3. GRB 940217: Broken power law photon spectra ("single detector mode").

Time interval (see Table 1)	Range MeV	normalization a photons/(cm^2 s MeV)	slope $\alpha_{\rm low}$	slope $\alpha_{\rm high}$	$E_{\rm break}$ MeV	$\chi^2_{\rm d.o.f.}$	d.o.f.
Full burst	0.6 − 10.0	$0.32^{+0.09}_{-0.06}$	$1.25^{+0.85}_{-1.20}$	$2.63^{+0.77}_{-0.35}$	$1.07^{+0.75}_{-0.35}$	16.2	18
Peak #1	0.6 − 10.0	$0.68^{+0.17}_{-0.17}$	$1.40^{+0.73}_{-1.20}$	$3.25^{+2.55}_{-0.55}$	$1.22^{+0.98}_{-0.37}$	13.6	15
Peak #4	0.6 − 10.0	$1.80^{+0.20}_{-0.40}$	$1.13^{+0.97}_{-1.10}$	$2.59^{+0.45}_{-0.19}$	$1.00^{+1.00}_{-0.24}$	29.3	30

Note: Errors on fit parameters are 90% confidence intervals (1.6σ).

Table 4. GRB 940217: Single power law photon spectra ("double scatter mode") obtained in the 0.75 − 30 MeV range.

Time interval (see Table 1)	normalization a photons/(cm^2 s MeV)	slope α	Π
Full burst	$0.38^{+0.03}_{-0.03}$	$2.61^{+0.11}_{-0.11}$	0.52
Peak #1	$0.93^{+0.11}_{-0.11}$	$3.02^{+0.22}_{-0.20}$	0.32
Peak #2	$0.12^{+0.08}_{-0.06}$	$3.03^{+1.56}_{-0.90}$	0.90
Peak #3	$0.60^{+0.11}_{-0.10}$	$2.68^{+0.28}_{-0.26}$	0.18
Peak #4	$2.31^{+0.44}_{-0.39}$	$2.63^{+0.27}_{-0.25}$	0.82
Peak #5	$0.27^{+0.06}_{-0.05}$	$2.44^{+0.31}_{-0.27}$	0.59
Peak #6	$0.13^{+0.06}_{-0.05}$	$3.45^{+1.21}_{-0.85}$	0.60

Note: Errors on fit parameters are 90% confidence intervals (1.6σ).
Note: Probability Π (column 5): see text.

COMPTEL operating modes. Note that the break observed in "single detector mode" (Figure 4) is just at the low energy boundary of the telescope spectrum shown in Figure 5. The best–fit power law slopes derived from all data in both operating modes are shown for comparison in Figure 6. The telescope data in Figure 6 strengthen our conclusion made above, that the spectral slopes of the individual peaks are significantly different. In addition, the overall trend of hard–to–soft evolution as indicated by the hardness ratios (Figure 3) can be confirmed.

Finally, we have investigated whether our data show a correlation between hardness and intensity. As independent variable ("intensity") we use for each of the individual peaks #1 to #6 background subtracted counts obtained in the "single detector mode" low range (0.3 − 1.5 MeV). The dependant variable ("hardness") is given by

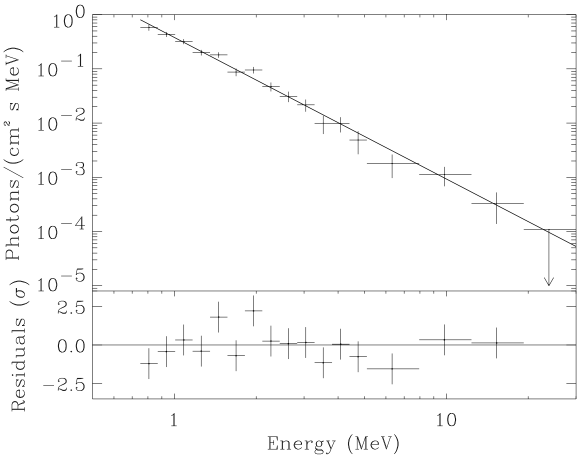

Fig. 5. Photon spectrum of GRB 940217 (full burst, 162 s duration) obtained in "double scatter mode". The best–fit single power law to the 0.75 – 30.0 MeV data is shown with $a = 0.38 \pm 0.03$ photons/(cm^2 s MeV) and slope $\alpha = 2.61 \pm 0.11$.

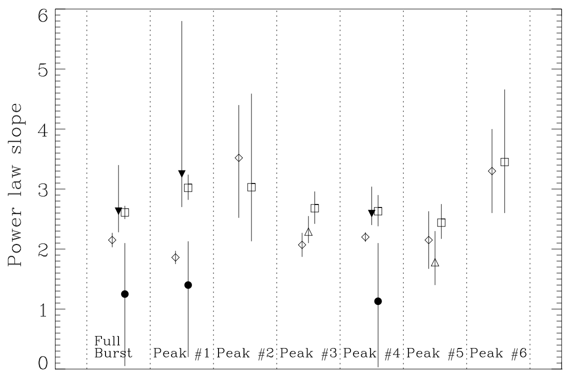

Fig. 6. GRB 940217: Best–fit power law slopes (α) for full burst and for peaks #1 to #6 obtained in "single detector mode" and "double scatter mode" (see Tables 2, 3, 4). *Single power law:* Diamonds: "single detector mode" low range 0.3 – 1.5 MeV. Open triangles: "single detector mode" high range 0.6 – 10.0 MeV. Squares: "double scatter mode" (telescope) 0.75 – 30 MeV. *Broken power law:* Filled circles: "single detector mode" high range 0.6 – 10.0 MeV below break energies at around 1 MeV. Filled triangles: "single detector mode" high range 0.6 – 10.0 MeV above break energies at around 1 MeV. Error bars are described by 90% confidence intervals.

the best–fit power law slopes per peak (fit energy range 0.3 – 1.5 MeV), as shown in Table 2 and Figure 6. A least squares fit to the data shows no significant deviation ($<1\sigma$) from a line of zero slope, indicating that the data are not correlated.

Comparison with other instruments In Figure 7 we have compiled the COMPTEL photon spectra (see above) together with the results from EGRET and BATSE data (Hurley et al. 1994c). The COMPTEL data cover the first 162 s of the burst event, while the EGRET and BATSE data were obtained during the first 180 s of the burst (Hurley et al. 1994c). The COMPTEL data do not show significant emission beyond 162 s, so that the results are comparable. The COMPTEL "single detector mode" data (see Figure 4) and "double scatter mode" data (see Figure 5) are shown again in Figure 7 as plain crosses and cover the energy range 0.3 – 30 MeV. The best–fit photon spectra to the COMPTEL data are given above (Figures 4 and 5). The best–fit photon spectrum obtained by the BATSE spectroscopy detectors (SD), covering the energy range 41 keV – 2.961 MeV (data = crosses with squares), is given by dN/dE = $(1.95 \pm 0.02) \times 10^{-2}$ (E/100 keV)$^{-1.215\pm0.02}$ $\times$ exp(–E/(838±63) keV) photons/(cm^2 s keV), and is shown as a solid line in Figure 7. The spectrum obtained by the EGRET total absorption shower counter (TASC) covers the energy range 0.9 – 200 MeV and the data (crosses with diamonds) are described by a single power law (dashed curve) with normalization $a = (3.6 \pm 0.26) \times 10^{-4}$ photons/(cm^2 s keV) at 1 MeV and slope $\alpha = 2.50 \pm 0.08$. The best–fit to the EGRET spark chamber data covers the energy range 30 – 4000 MeV and is given by a power law $(2.91 \pm 0.97) \times 10^{-7} \times$ (E/128 MeV)$^{-2.08\pm0.56}$ photons/(cm^2 s MeV) and is shown as dashed–dotted curve in Figure 7.

The overall consistency of the observations from three different instruments on board CGRO is remarkably good, in particular the consistency with COMPTEL and BATSE at energies below 1 MeV and consistency with COMPTEL and EGRET TASC. We note that the BATSE SD best–fit is somewhat low close to its sensitivity limit at ~3 MeV and that the EGRET spark chamber best–fit is not a high energy extrapolation of the TASC MeV data. This is also directly evident from the EGRET data points shown by Hurley et al. (1994c) and may indicate a possible turnover in the spectrum at around 50 MeV.

3.2.3. Fluence

GRB 940217 was the strongest burst observed so far by COMPTEL (see Hanlon et al. 1994 for a discussion on earlier events observed by COMPTEL): using the fit results for the full burst (162 s duration) from Tables 2 and 3 we obtain a fluence S($>$ 0.3 MeV) = 2.03 $\times 10^{-4}$ erg cm^{-2}.

3.2.4. Line emission

All individual "single detector mode" spectra accumulated during the burst emission (162 s) have been visually inspected in both ranges (0.3 – 1.5 MeV and 0.6 – 10.0 MeV, 32 spectra per range) and no significant emission or absorption feature had been detected. In addition, as described above, all spectra could be modelled using continuum spectra not requiring an additional spectral component (e.g. line feature). This negative result adds to the

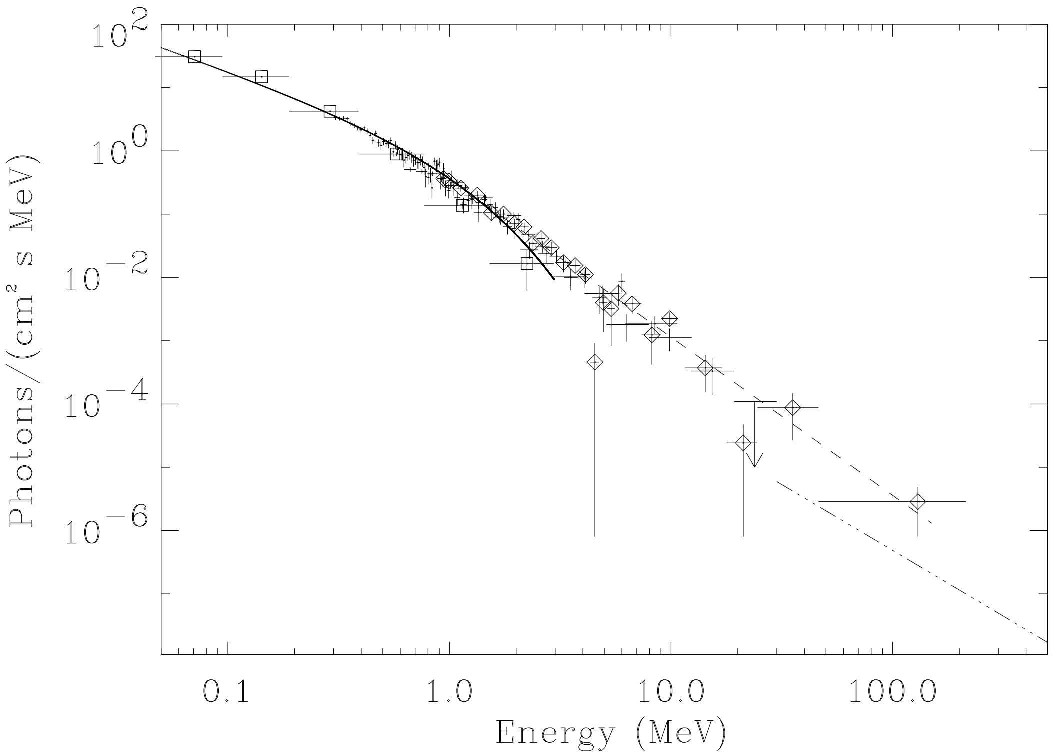

Fig. 7. Photon spectrum of GRB 940217 obtained with COMPTEL (data of both modes = plain crosses), BATSE (data = crosses with squares, best–fit = solid line), EGRET TASC (data = crosses with diamonds, best–fit = dashed line), and EGRET spark chamber (best–fit = dashed–dotted line). The BATSE and EGRET results are taken from Hurley et al. (1994c). See text for details.

earlier results that none of the COMPTEL gamma–ray bursts analysed so far (Winkler et al. 1992b, Hanlon et al. 1994 and references therein) have revealed any significant line feature in the data.

3.3. Spatial analysis

3.3.1. Location and counterparts

Imaging events observed in the "double scatter mode" are analysed in a three–dimensional data space defined by the two co–ordinates of the Compton scatter direction and the Compton scatter angle which are defined – via the Compton formula – by the electron rest mass energy and the energy deposits in the upper and lower detector arrays, respectively (Schönfelder et al. 1993). Using maximum likelihood analysis (de Boer et al. 1992) this data space is searched for the presence of a point source. This procedure reveals both the significance of the source and its position on the sky.

For GRB 940217, a total of 743 "double scatter mode" events (source and background) were selected from the full burst time interval (Table 1) with standard event selection filters for time–of–flight, pulse shape discrimination, energy deposits in both detector arrays and Compton scatter angle (Schönfelder et al. 1993). These events were binned into the three–dimensional data space with bin size of 1° for scatter direction and 2° for Compton scatter angle. A three–dimensional source model was generated by simulating a source power law (E^{-2}) spectrum, and a background model was generated by sampling events from orbit conditions similar to those during the burst observations. These correspond to events from a time interval taken 15 orbits ($\sim$ 1 day) after the event. After 15 orbits the spacecraft is again located at the same position above the earth surface (same suborbital points), so that the orbital radiation environment is nearly identical. Source and background scale factors were allowed to vary independently in order to fit the observed distribution of events as the maximum likelihood ratio was computed for each position on the sky around the most likely position. The parameters of interest from the resulting COMPTEL sky map of maximum likelihood ratios are: peak value = 18.8σ, peak position: (α_{2000}, δ_{2000}) = (30.1°, 3.1°), and (l,b) = (154.49°, - 55.49°). The COMPTEL location of this burst was communicated via the Rapid Response Network (Kippen et al. 1993, 1994a) $4^{\rm h}$ $15^{\rm min}$ after receipt of the BATSE trigger to initiate a world wide search for optical and radio counterpart emission. Radio observations began as soon as $5^{\rm h}$ after the burst emission. So far no positive detections of quiescent or fading counterparts have been reported (McNamara et al. 1995).

An *improved* burst location can be obtained by using the COMPTEL data together with results from the IPN (Interplanetary Network) triangulation arc (Hurley et al. 1994b). The annulus passes through the COMPTEL 1.8σ confidence contour, and the COMPTEL derived position (above) is only 0.9° away from the IPN annulus at its closest approach. A combined COMPTEL/IPN localization has been calculated by evaluating the COMPTEL maximum likelihood ratios at several points along the IPN annulus. Bicubic interpolation was used due to the coarse COMPTEL binning ($\sim$ degree). The most likely COMPTEL/IPN position is where the COMPTEL maximum likelihood ratio is highest along the arc. The confidence contours (1σ, 2σ, 3σ) have been determined from those values in the maximum likelihood map where the value of the maximum likelihood ratio (362.2) has dropped by 1, 4 and 9. The width of the IPN annulus is negligible compared to the intrinsic spatial resolution of COMPTEL. The parameters of interest from the resulting COMPTEL/IPN sky map of maximum likelihood ratios are: peak position: $(\alpha_{2000}, \delta_{2000}) = (29.5°, 3.8°)$, confidence intervals: 1σ: $-\,0.37° \rightarrow +\,0.28°$, 2σ: $-\,0.66° \rightarrow +\,0.56°$, 3σ: $-\,0.94° \rightarrow +\,0.84°$. The sky map containing the most likely COMPTEL/IPN position is shown in Figure 8.

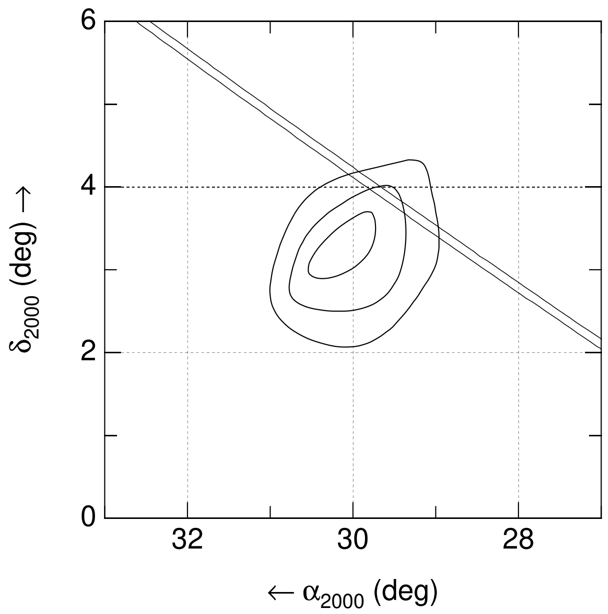

Fig. 8. Maximum likelihood sky map showing the most likely position of GRB 940217 using COMPTEL imaging and IPN triangulation. The contours denote confidence intervals of 1σ, 2σ, and 3σ, respectively. The burst position is at $(\alpha_{2000}, \delta_{2000}) = (29.5°, 3.8°)$.

3.4. "Post–burst" emission

During the entire burst emission (162 s) high energy photons (up to 4.4 GeV) were reported by the EGRET instrument (Hurley et al. 1994a, 1994c). Most importantly, on the subsequent orbit of CGRO, $\sim$ 90 minutes later, EGRET detected 10 photons in its spark chamber – one with an energy of 18.4 GeV – within a 20 minute time interval from the burst region. In addition, the EGRET NaI calorimeter (TASC) detected during that "post–burst" interval (from $0^{\rm h}\,20^{\rm m}$ to $0^{\rm h}\,40^{\rm m}$ (UT) during TJD 9401) fluxes of $\sim 1.2 \times 10^{-3}$ and $\sim 1.4 \times 10^{-4}$ photons/(cm^2 s MeV) in the energy bands 1.07 – 6.1 MeV and 6.1 – 26.2 MeV, respectively (Hurley et al. 1994c).

During the CGRO orbit, subsequent to the event of GRB 940217, the "source" was visible to COMPTEL (i.e. within the FOV) on 1994 February 18 (TJD 9401), from 754 s (UT) until 3408 s (UT), a time interval which included the 20 minute interval of EGRET detection.

We have compared a time series of counts in "single detector mode" from both ranges (0.3 – 1.5 MeV and 0.6 – 10.0 MeV) accumulated during this "source visibility" period with data of same length accumulated 15 orbits ($\sim 8.4 \times 10^4$ s) later (i.e. representing a nearly identical orbital radiation environment). These datasets were subtracted from each other, any residual flux should indicate the presence of "post–burst" emission in the COMPTEL "single detector" energy range (0.3 – 10.0 MeV). During the "visibility" period of the source – i.e. the time interval corresponding to the positive EGRET detection of "post–burst" emission – we do not detect any significant signal in our 0.3 – 10.0 MeV data. The 2σ upper limits are 2.3 $\times 10^{-2}$ and 8.9 $\times 10^{-4}$ photons/(cm^2 s MeV) in the low range 0.3 – 1.5 MeV and high range 0.6 – 10.0 MeV, respectively.

Our method was cross-checked using a time interval during which the source was occulted (from 1994 February 17 (TJD 9400), 84900 s (UT) to 1994 February 18 (TJD 9401), 754 s (UT)) and again compared with data from a time interval of the same length, taken 15 orbits later. Subtraction of those datasets (" source occultation") resulted in residual counts compatible with zero.

"Double scatter mode" (telescope) data have also been searched for emission in the "post–burst" time interval (identical to the one as used by EGRET) by examining both the sky map (background subtracted events selected from a $\sim 10°$ sky region around the burst position) and the lightcurve. We used a background estimate from a time series of events accumulated 15 orbits later. We did not find any significant excess in the lightcurve, and the derived image did not show any excesses above 2σ. The 2σ upper limits on the integrated flux in the 1.07 – 6.1 MeV and 6.1 – 26.2 MeV bands are 7.34×10^{-4} and 8.22 $\times\ 10^{-5}$ photons/(cm^2 s MeV), respectively.

In Figure 9 we compare our upper limits with the EGRET/TASC detections. We have also included in Figure 9 the best–fit power law to the EGRET (30 MeV – 30 GeV) spark chamber data extrapolated down to the COMPTEL energies (dashed line), and extreme ranges of this fit as given by the best–fit errors (dotted lines) (Hurley et al. 1994c). The best–fit power law shown is given[1] by $(1.03 \pm 0.4) \times 10^{-7} \times (E/86\ \mathrm{MeV})^{-2.83 \pm 0.64}$ photons/(cm^2 s MeV).

We conclude that our COMPTEL upper limits are marginally consistent with the EGRET/TASC detections. All data (< 30 MeV) are consistent with the low energy extrapolation of the best–fit power law obtained for the EGRET spark chamber data (30 MeV – 30 GeV).

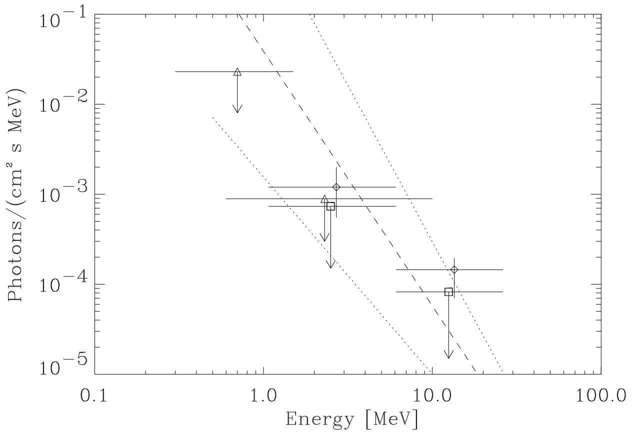

Fig. 9. "Post–burst" emission of GRB 940217. COMPTEL 2σ upper limits are shown ("single detector mode" = triangles, "double scatter mode" = squares) together with EGRET/TASC detections (diamonds and 1σ error bars) and the extrapolated best–fit power law to EGRET spark chamber data (30 MeV – 30 GeV, dashed and dotted lines). EGRET data are taken from Hurley et al. 1994c. See text for details.

4. Discussion

4.1. Spectral breaks

We have observed spectral breaks at around 1 MeV in most of the strong peaks of GRB 940217. In addition, the well known phenomenon of hard–to–soft evolution during MeV bursts (Norris et al. 1986, Winkler et al. 1992b, Schaefer et al. 1992a, Schaefer et al. 1992b, Hanlon et al. 1994) was again observed. The softening has been observed within peaks and also from peak to peak during the burst emission. Spectral breaks should be a diagnostic in the continuum of a photon spectrum, being related to optical depth effects in the MeV region. These breaks can be caused by several mechanisms including e^+e^- – pair creation from γ–γ interaction or from single photon interaction with strong (> 10^{12}G) magnetic fields, or photon splitting (see below).

4.2. Distance

A *lower limit* to the distance of GRB 940217 can be obtained by computing the angular offset ("parallax") from the IPN annulus at all COMPTEL sky bins and comparing each maximum likelihood ratio at each bin to the ratio obtained at the most likely COMPTEL/IPN position (Connors et al. 1992, Ryan et al. 1994). However, it is assumed that the offset of the most likely position from the IPN arc (Figure 8) of $\sim 0.5°$ reflects the experimental systematic error. We can further constrain our data by considering the fact that a "nearby" source can only result in an annulus with a true radius smaller than the one deduced from the IPN timing differences (which assumes a source at infinity). Using a Ulysses/CGRO distance of 3.038 AU and the IPN annulus radius of 69.33° centered on $(\alpha_{2000}, \delta_{2000}) = (21^{\mathrm{h}}\ 54.9^{\mathrm{m}}, +51°\ 57')$ at the time of the burst event (Hurley et al. 1994b), the significances of the IPN offsets have been evaluated and we derive a 2σ lower limit on the distance to GRB 940217 of 145 AU.

In order to derive an *upper limit* on the distance we use information on high energy emission together with temporal fine structure (following Ryan et al. 1994). Temporal fine structure has been described in Section 3.1 and the shortest peaks occur in peak #4 (see Figure 2) with a full width of ~ 0.1 s. This leads to a maximum size (2c×0.1s) of 6×10^4 km of the emitting site. Although EGRET reported energies (Hurley et al. 1994c) to be much higher, derivation of a distance limit requires information on temporal variations as provided only by COMPTEL. Concerning high energy emission, we observe during peak #4 a power law spectrum in the "single detector mode" data (6 s binning) with a break at 1 MeV indicating an opacity $\tau \sim 1$. However, the spectra obtained in both observing modes for peak #4 do not sharply cut off above 1 MeV and the power law spectrum (as observed in "double scatter mode") is not attenuated up to 4.4 MeV (> 3σ significance). Attenuation of the high energy flux (E > 1 MeV) should be expected if the burst source emits its radiation isotropically and homogeneously at large distances (Schmidt 1978) because of γ–γ interaction (e^+e^- – pair creation). Following Schmidt (1978) this leads to an upper limit on the distance of the homogenous and isotropic burst emitting site of 5.3 kpc using the break energy (~ 1 MeV) as an indicator for opacity $\tau \sim 1$ during peak #4. Using the highest significant (> 3σ) energy (4.4 MeV) of peak #4 as observed in the telescope spectrum, we obtain 1.3 kpc as limit of the distance to a homogenous isotropically radiating burst (site). For the full burst emission (162 s), the upper limit to the distance is 11.7 kpc (break energy ~ 1 MeV).

[1] Note that the best–fit power law as given in the caption of Figure 3 of Hurley et al. (1994c) is erroneously too low by a factor of 10 (Hurley 1995, priv. communication).

If we consider beaming effects, however, the upper limit on the distance can be much larger. In fact, we can assume any cosmological distance and subsequently calculate how much beaming must be present at the source site in order not to see attenuation of high energy emission due to γ–γ interaction.

Using again peak #4 (slope = 2.63) and following Baring (1994, equation 15), we calculate a lower limit of the Lorentz beaming factor $\gamma_B = 27$ (for energy E = 4.4 MeV) and $\gamma_B = 18$ (1 MeV) for an assumed distance of 1 Gpc (z = 0.27).

Our observation of fast temporal variation at high (> 1 MeV) energies require a Lorentz factor of $\gamma_B > 18$. We conclude (following Baring 1994), that with such beaming, the cut–off energy for photon opacity is blue–shifted to $E \geq \gamma_B m_e c^2 = 9.2$ MeV to avoid Comptonization which is not observed in our data. Our observed spectral breaks are therefore too low in energy, which means that either GRB 940217 is closer than 1 Gpc, or the break is not produced by γ–γ interaction, but by a different process, e.g. single photon interaction with strong ($> 10^{12}$G) magnetic fields leading to pair creation, or photon splitting (cf. Baring 1990).

4.3. Lightcurve

Properties of extragalactic GRB's have been modelled recently in the frame of extragalactic radio sources using a precessing relativistic e^+e^- – beam with a Lorentz bulk factor of $\gamma_B \sim 10$ (Roland et al. 1994). These authors assume that the gamma–ray emission of the ejected e^+e^- – component has a non–thermal origin and is a product of e^+e^- – annihilation plus inverse–Compton losses. Anisotropic emission is a consequence of relativistic motion of the e^+e^- – component. Assuming that a compact object revolves around a central black hole at ~3 Schwarzschild radii, the perturbation beam model (Roland et al. 1994) predicts a typical time scale between peaks in the lightcurve of GRB's corresponding to the orbital rotation frequency of the compact object. From Figures 1 and 2, the typical time scale between peaks is seen to be of the order of 10 s, yielding a period of perturbation of the beam of a few 10^2 s and a central black hole mass of $\sim 10^4$ $M_\odot$. Gravitational interaction between the black hole and the revolving compact object would – according to this model – result in a perturbation of the accretion disk thereby inducing instabilities with a period of a few 10^2 s. Perturbation of the accretion disk will then produce a precession of the jet via its magnetic field lines, frozen in the plasma of the disk which might produce late events as seen by EGRET.

5. Conclusions

COMPTEL observations of GRB 940217 have shown that this event is very strong, complex, and long lasting. The burst consists of several peaks with short temporal fluctuations. Hard–to–soft spectral evolution has been observed throughout the burst event and also from peak to peak. The photon spectra obtained within the peaks can be modelled by single power law spectra and by broken power laws with break energies at around 1 MeV. No significant line emission is detected in any of the recorded spectra. Precise location of the event has been obtained through direct COMPTEL MeV imaging in combination with timing analysis by the Interplanetary Network. The COMPTEL upper limits obtained during the "post–burst" emission are marginally consistent with the detections as reported by EGRET. Distance limits to GRB 940217 have been derived assuming homogenous and isotropic emission as well as beamed emission. The lower limits obtained for the Lorentz beaming factor require that either the burst is closer than 1 Gpc, or that γ–γ interaction is not the mechanism responsible to produce spectral breaks.

Acknowledgements. We thank the BATSE team for the burst trigger, B. Dingus who provided us with the EGRET data prior to publication, and D. Band for the BATSE data. The COMPTEL project is supported by the German government through DARA grant 50 QV 9096, by NASA under contract NAS5–26645 and by the Netherlands Organisation for Scientific Research (NWO). K.S. O'Flaherty acknowledges receipt of a research fellowship from ESA. L.O. Hanlon acknowledges the Education Programme of the European Community for a fellowship and ESA/ESTEC for facilities.

References

Baring, M. 1990, MNRAS 244, 49
Baring, M. 1994, ApJS 90, 899
de Boer, H., Bennett, K., Bloemen, H. et al. 1992, in: Data Analysis in Astronomy IV (Eds.: Di Gesú, V. et al.), Plenum Press, New York, p. 241
Cash, W.C. 1976, ApJ 228, 939
Collmar, W., Bennett, K., Bloemen, H. et al. 1992, A&AS 97, 71
Connors, A., Aarts, H., Bennett, K. et al. 1992, A&AS 97, 75
Hanlon, L.O., Bennett, K., Collmar, W. et al. 1994, A&A 285, 161
Hurley, K., Boer, M., Niel, M. et al. 1994a, BAAS (184th Meeting of the AAS), paper 15.01
Hurley, K., Bertsch, D., Cline, T. et al. 1994b, IAUC 5940
Hurley, K., Dingus, B., Mukherjee, R. et al. 1994c, Nature 372, 652
Kippen, R.M., Macri, J., Ryan, J. et al. 1993, in: *Compton* Gamma–Ray Observatory (Eds. Friedlander, M., Gehrels, N., Macomb, D.), AIP Conf. Proc. 280, 823
Kippen, R.M., Macri, J., Ryan, J. et al. 1994a, IAUC 5937
Kippen, R.M., Connors, A., McConnell, M. et al. 1994b, 30th COSPAR meeting, in press
Lampton, M., Margon, B., and Bowyer, S. 1976, ApJ 208, 177
McNamara, B., Harrison, T., Ryan, J. et al. 1995: BAAS (185th Meeting of the AAS), paper 15.03
Norris, J., Share, G., Messina, D. et al. 1986, ApJ 301, 213
Roland, J., Frossati, G., and Teyssier, R. 1994, A&A 290, 364

Ryan, J., Bennett, K., Collmar, W. et al. 1994, ApJ 422, L67
Schaefer, B., Teegarden, B., Cline, T. et al. 1992a, ApJ 393, L51
Schaefer, B., Teegarden, B., Cline, T. et al. 1992b, in: Gamma–Ray Bursts (Eds.: Paciesas, W. & Fishman, G.), AIP Conf. Proc. 265, 180
Schmidt, W. 1978, Nature 271, 525
Schönfelder, V., Aarts, H., Bennett, K. et al. 1993, ApJS 86, 657
Varendorff, M.G., Bennett, K., de Boer, H. et al. 1992, in: Gamma–Ray Bursts (Eds.: Paciesas, W. & Fishman, G.), AIP Conf. Proc. 265, 77
Winkler, C., Bennett, K., Bloemen, H. et al. 1992a, A&A 255, L9
Winkler, C., Bennett, K., Hanlon, L. et al. 1992b, in: *Compton* Gamma–Ray Observatory (Eds. Friedlander, M., Gehrels, N., Macomb, D.), AIP Conf. Proc. 280, 845
Winkler, C., Bennett, K., Bloemen, H. et al. 1992c, in: Gamma–Ray Bursts (Eds. Paciesas, W. & Fishman, G.), AIP Conf. Proc. 265, 22

This article was processed by the author using Springer-Verlag LaTeX A&A style file *L-AA* version 3.